A new method to estimate ionospheric electric fields and currents using data from a local ground magnetometer network

H. Vanhamäki, O. Amm

▶ **To cite this version:**

H. Vanhamäki, O. Amm. A new method to estimate ionospheric electric fields and currents using data from a local ground magnetometer network. Annales Geophysicae, 2007, 25 (5), pp.1141-1156. hal-00318323

HAL Id: hal-00318323
https://hal.science/hal-00318323

Submitted on 4 Jun 2007

HAL is a multi-disciplinary open access archive for the deposit and dissemination of scientific research documents, whether they are published or not. The documents may come from teaching and research institutions in France or abroad, or from public or private research centers.

L'archive ouverte pluridisciplinaire **HAL**, est destinée au dépôt et à la diffusion de documents scientifiques de niveau recherche, publiés ou non, émanant des établissements d'enseignement et de recherche français ou étrangers, des laboratoires publics ou privés.

Ann. Geophys., 25, 1141–1156, 2007
www.ann-geophys.net/25/1141/2007/
© European Geosciences Union 2007

Annales Geophysicae

A new method to estimate ionospheric electric fields and currents using data from a local ground magnetometer network

H. Vanhamäki and O. Amm

Finnish Meteorological Institute, Space Research Unit, P.O. Box 503, 00101 Helsinki, Finland

Received: 8 February 2007 – Revised: 26 April 2007 – Accepted: 7 May 2007 – Published: 4 June 2007

Abstract. In this study we present a new method to estimate ionospheric electric fields and currents using ground magnetic recordings and measured or modeled ionospheric electric conductivity as the input data. This problem has been studied extensively in the past, and the standard analysis technique for such a set of input parameters is known as the KRM method (Kamide et al., 1981). The new method presented in this study makes use of the same input data as the traditional KRM method, but differs significantly from it in the mathematical approach that is used. In the KRM method one tries to find such a potential electric field, that the resulting current system has the same curl as the ionospheric equivalent currents. In the new method we take a different approach, so that we determine such a curl-free current system that, together with the equivalent currents, it is consistent with a potential electric field. This approach results in a slightly different equation, that makes better use of the information contained in the equivalent currents. In this paper we concentrate on regional studies, where the (unknown) boundary conditions at the borders of the analysis area play a significant role in the KRM solution. In order to overcome this complication, we formulate a novel numerical algorithm to be used with our new calculation method. This algorithm is based on the Cartesian elementary current systems (CECS). With CECS the boundary conditions are implemented in a natural way, making regional studies less prone to errors. We compare the traditional KRM method and our new CECS-based formulation using several realistic models of typical meso-scale phenomena in the auroral ionosphere, including a uniform electrojet, the Ω-bands and the westward traveling surge. It is found that the error in the CECS results is typically about 20%–40%, whereas the errors in the KRM results are significantly larger.

Keywords. Ionosphere (Auroral ionosphere; Electric fields and currents; Instruments and techniques)

Correspondence to: H. Vanhamäki
(heikki.vanhamaki@fmi.fi)

1 Introduction

Determination of ionospheric electrodynamic parameters from direct or indirect measurements is a fundamental task in ionospheric physics. Over the years several methods have been developed to estimate various parameters or their combinations from different sets of measured or modeled data (see e.g. Untiedt and Baumjohann, 1993; or Amm et al., 2003, for references). In this paper we present a new method to estimate ionospheric electric fields and currents using ground magnetic recordings and ionospheric electric conductivity as the input data. This problem has been studied extensively in the past, especially by Kamide and co-workers (Kamide et al., 1981; Murison et al., 1985, and references therein). The standard analysis technique for this set of input parameters is known as the KRM method developed by Kamide et al. (1981).

The ground magnetic data is most conveniently used in form of ionospheric equivalent currents. By definition, they are divergence-free horizontal sheet currents, that produce the same magnetic field below the ionosphere as the real (unknown) 3-dimensional current system. Equivalent currents can be calculated using standard techniques, like spherical harmonic analysis (Chapman and Bartels, 1940) in global scales and spherical cap harmonic analysis (Haines, 1985) in regional studies, or elementary current method (Amm and Viljanen, 1999; Pulkkinen et al., 2003) in all scales. The other input parameter, distribution of ionospheric Pedersen and Hall conductivities, is more difficult to estimate reliably. Conductivities may be obtained from satellite or all-sky camera images (e.g. Lummerzheim et al., 1991; Janhunen, 2001; Aksnes et al., 2005), but the temporal and spatial coverage is often insufficient and a number of unknown model parameters or empirical relations need to be assumed. Also statistical models like Fuller-Rowell and Evans (1987) may be used, but they are not very accurate during disturbed conditions. If no other measurement are available, a rough estimate of the ionospheric conductances may be obtained from the ground magnetic data, as done by Ahn et al. (1998).

Published by Copernicus GmbH on behalf of the European Geosciences Union.

The new method presented in this article makes use of the same input data as the traditional KRM method, but differs significantly from it in the mathematical approach. In the KRM method one tries to find such a potential electric field, that the resulting current system has the same curl as the ionospheric equivalent currents. Once this electric field is obtained, also the field aligned currents (FAC) and corresponding curl-free horizontal currents (which are magnetically invisible below the ionosphere) may be calculated. In the new method this approach is reversed, so that we determine such a curl-free current system that, together with the equivalent currents, it is consistent with a potential electric field. This approach results in a slightly different equation, that makes better use of the information contained in the equivalent currents. The mathematical formulation of both the KRM method and our new approach are presented in more detail in Sect. 2.

In the past the KRM method has been used mostly in global or semi-global scales, but in this study we concentrate on regional analysis. In these smaller scales the (unknown) boundary conditions at the borders of the analysis area affect the KRM solution significantly, as was shown by Murison et al. (1985) and discussed further in Sect. 2.1. In Sect. 3 we formulate a novel numerical algorithm to be used with our new calculation method. This algorithm is based on the Cartesian elementary current systems (CECS), that were introduced by Amm (1997). With the use of CECS the boundary conditions can be implemented in a very convenient and natural way, which makes regional studies less prone to errors. We compare the traditional KRM method and our new CECS based formulation first in a simple electrojet situation in Sect. 4. In Sect. 5 we continue the comparisons using two realistic data based models of typical meso-scale phenomena in the auroral ionosphere, namely the Ω-bands and the westward traveling surge (WTS). Section 6 is summary and conclusions.

2 Theory

In this section we first give a short review of the KRM method and then introduce our own, somewhat different approach to solving the same problem. We obtain a partial differential equation that we solve numerically using the Cartesian elementary current systems (CECS), introduced in Sect. 3.1.

In this study we use the thin-sheet approximation, i.e. we assume that ionospheric horizontal currents flow at a thin spherical layer at about 100 km altitude. We concentrate on local scale studies, where we use a Cartesian coordinate system with x-axis pointing North, y-axis East and z-axis down. The Earth's magnetic field is assumed to be parallel to the z-axis, which is a reasonable approximation near the auroral oval. Furthermore, we assume that the electric field parallel to the magnetic field is zero due to the high conductivity in this direction.

2.1 The KRM method

Kamide et al. (1981) developed the KRM method for determining ionospheric electric field and currents in situations where estimates of height-integrated ionospheric Pedersen and Hall conductances, Σ_P and Σ_H, together with ground magnetic measurements are available. From the ground magnetic measurements one can obtain the ionospheric equivalent current density $\boldsymbol{J}_{eq}$ using standard techniques (e.g. Chapman and Bartels, 1940; Haines, 1985; Amm and Viljanen, 1999).

For a vertical background magnetic field, $\boldsymbol{J}_{eq}$ is equal to the divergence-free part of the true ionospheric current density $\boldsymbol{J}$ (see e.g. Untiedt and Baumjohann, 1993), so that

$$\nabla \times \boldsymbol{J}_{eq} = \nabla \times \boldsymbol{J}. \tag{1}$$

The ionospheric electric field $\boldsymbol{E}$ is assumed to be given by a potential ϕ as

$$\boldsymbol{E} = -\nabla\phi. \tag{2}$$

In the KRM method Eqs. (1) and (2) are used together with ionospheric Ohm's law

$$\boldsymbol{J} = \Sigma_P \boldsymbol{E} + \Sigma_H \hat{\boldsymbol{e}}_z \times \boldsymbol{E} \tag{3}$$

to obtain a differential equation for the electric potential,

$$\Sigma_H \nabla^2\phi + \nabla\Sigma_H \cdot \nabla\phi + (\nabla\Sigma_P \times \nabla\phi)_z = -(\nabla \times \boldsymbol{J}_{eq})_z. \tag{4}$$

If ionospheric conductances and equivalent currents are know, the electric potential can be solved. This gives a complete solution of the ionospheric electric properties, for the electric field is given by Eq. (2), horizontal currents are obtained from Ohm's law and FAC are given by current continuity,

$$j_\parallel = \nabla \cdot \boldsymbol{J}. \tag{5}$$

If Eq. (4) is solved globally, we only have to fix the zero level of potential. Also in semi-global studies, that cover either the northern or southern auroral regions, boundary conditions of the electric potential are not problematic, as they have to be specified only at the mid-latitudes, where the electric field is rather small in any case. However, in meso-scale studies, covering areas of few hundred or at most few thousand km across, boundary conditions play an important role. This was demonstrated by Murison et al. (1985), who studied a situation where the Harang discontinuity was present over northern Scandinavia. They found that in the regional analysis the electric field, and consequently also the currents, depend strongly on the boundary conditions. This severely limits the use of the KRM method in regional studies. Recently Kamide et al. (2003) have developed a local variant of the KRM method, where the KRM is used in

areas of good data coverage and required boundary conditions are obtained using the AMIE technique (Assimilative Mapping of Ionospheric Electrodynamics, Richmond and Kamide, 1988). This allows one to use the local KRM in a rather straightforward manner. However, it should be kept in mind that in absence of global data coverage AMIE gives results that are mostly based on statistical models, and therefore the obtained boundary conditions may not be very accurate.

Probably the greatest uncertainties in the KRM results are caused by uncertainties in the input conductance distributions (Murison et al., 1985). Two-dimensional ionospheric conductance distributions are quite difficult to obtain from direct measurements. Large scale conductance distributions may be derived from satellite or all-sky camera images (e.g. Lummerzheim et al., 1991; Janhunen, 2001; Aksnes et al., 2005), statistical models (e.g., Fuller-Rowell and Evans, 1987) or the ground magnetic data (Ahn et al., 1998), as discussed in the Introduction.

2.2 Different approach

In the KRM method one tries to find such a potential electric field that the curl of the corresponding current density is equal to the curl of the equivalent currents. Another possible approach is to try to find such a curl-free current system that together with the equivalent currents it is consistent with a non-rotational potential electric field. This latter approach will now be developed.

As stated above, for a vertical background magnetic field, $\boldsymbol{J}_{eq}$ is equal to the divergence-free part of the true ionospheric current density $\boldsymbol{J}$. In this case the curl-free part of $\boldsymbol{J}$, together with associated FAC, is magnetically invisible below the ionosphere. These are good approximations even with moderate ($\chi \approx 75°$) inclinations of the main magnetic field (Untiedt and Baumjohann, 1993). Consequently we may write $\boldsymbol{J}$ as a sum of the equivalent currents and a potential part of the current,

$$\boldsymbol{J} = \boldsymbol{J}_{eq} - \nabla\Phi. \tag{6}$$

We can solve the electric field from Ohm's law as

$$\boldsymbol{E} = (\Sigma_P \boldsymbol{J} - \Sigma_H \hat{\boldsymbol{e}}_z \times \boldsymbol{J})/\Sigma^2, \tag{7}$$

where

$$\Sigma^2 = \Sigma_P^2 + \Sigma_H^2.$$

The condition $\nabla\times\boldsymbol{E}=0$ leads to a differential equation for the potential part of the current density,

$$\Sigma^2\Sigma_H\nabla^2\Phi + \boldsymbol{\beta}_1\cdot\nabla\Phi - (\boldsymbol{\beta}_2\times\nabla\Phi)_z = \\ = -\Sigma^2\Sigma_P(\nabla\times\boldsymbol{J}_{eq})_z + \boldsymbol{\beta}_1\cdot\boldsymbol{J}_{eq} - (\boldsymbol{\beta}_2\times\boldsymbol{J}_{eq})_z, \tag{8}$$

where

$$\boldsymbol{\beta}_1 = \Sigma^2\nabla\Sigma_H - \Sigma_H\nabla\Sigma^2$$
$$\boldsymbol{\beta}_2 = \Sigma^2\nabla\Sigma_P - \Sigma_P\nabla\Sigma^2.$$

The equation we obtained is similar in structure to Eq. (4). One significant difference is that in the KRM equation only $\nabla\times\boldsymbol{J}_{eq}$ appears, whereas now also the vector $\boldsymbol{J}_{eq}$ itself is needed. In a limited area $\boldsymbol{J}_{eq}$ may have a Laplacian part that has zero curl inside the analysis area. This part of $\boldsymbol{J}_{eq}$ does not contribute to the KRM solution, but it is included in Eq. (8).

When solving Eq. (8) we have to specify the conductances, so the same problems arise as in the KRM method. Furthermore, if Eq. (8) is solved in some limited area, we have to specify some boundary conditions for the curl-free part of the ionospheric current density. In Sect. 3 we present an algorithm based on the CECS, where the boundary conditions are handled in a natural and convenient manner.

It should be noted that in both methods, KRM and the new formulation, the electric field is assumed to be an irrotational potential field. Vanhamäki et al. (2007) have shown that in some very dynamical situations ionospheric self-induction creates significant induced rotational electric fields, that drive large horizontal currents and FAC. The induced rotational part of the electric field may be estimated from the time derivative of the equivalent currents (in a rather approximate way), as done in Vanhamäki et al. (2007). Consequently, we can estimate that part of the equivalent currents that is associated with the induced electric field, and subtract it from the total $\boldsymbol{J}_{eq}$ if necessary. This way we can obtain a more reliable estimate for the potential part of the electric field even in those cases where induction is important.

3 Numerical solution using elementary current systems

3.1 CECS

We can represent the ionospheric electric fields and currents by using special non-local vector basis functions, Cartesian Elementary Current Systems (CECS). CECS were introduced by Amm (1997) and although the name "CECS" refers to current systems, they can be used to represent any smooth enough 2-dimensional vector field in planar geometry. There are two different types of CECS, one is divergence-free (DF) and the other curl-free (CF). Together they form a complete set of basis functions. The elementary systems, illustrated in Fig. 1, are defined as

$$\boldsymbol{E}^{df} = \frac{V^{df}}{2\pi\rho'}\,\hat{\boldsymbol{e}}_{\phi_p} \tag{9}$$

$$\boldsymbol{E}^{cf} = \frac{V^{cf}}{2\pi\rho'}\,\hat{\boldsymbol{e}}_{\rho_p}. \tag{10}$$

Here $\rho'=\sqrt{(x-x_p)^2+(y-y_p)^2}$ is the distance between the observation point (x, y) and the CECS pole located at (x_p, y_p). Unit vectors $\hat{\boldsymbol{e}}_{\phi_p}$ and $\hat{\boldsymbol{e}}_{\rho_p}$ are given in the cylindrical coordinate system centered at the CECS pole. Constants

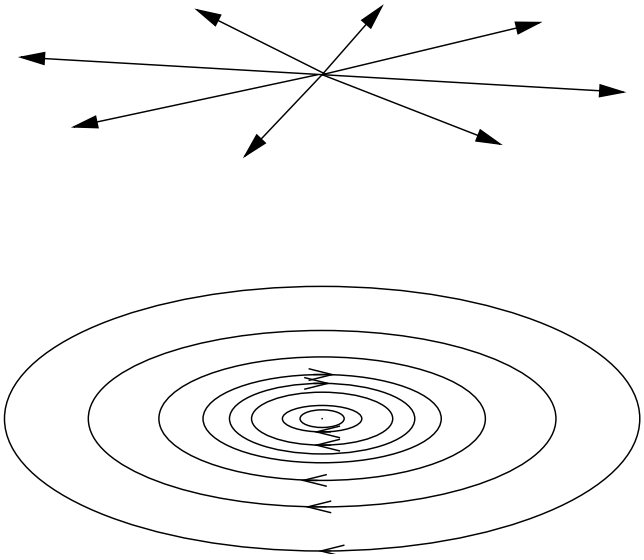

Fig. 1. Schematic presentation of curl-free (upper) and divergence-free (lower) Cartesian elementary current systems (CECS).

V^{cf} and V^{df} are called the scaling factors of the CF and DF CECS, respectively.

The elementary systems are defined in such a way, that the CF CECS has a Dirac δ-function divergence and the DF CECS a δ-function curl at its pole,

$$\nabla \cdot \boldsymbol{E}^{cf} = V^{cf}\,\delta(x-x_p)\,\delta(y-y_p)$$

$$(\nabla \times \boldsymbol{E}^{df})_z = V^{df}\,\delta(x-x_p)\,\delta(y-y_p).$$

By placing a sufficient number of CF and DF CECS at different locations of the plane, one can construct any 2-dimensional vector field from its sources and curls, in accordance with Helmholtz's theorem. When CECS are used to represent ionospheric currents, the divergence of the CF CECS at its pole is interpreted as a vertically flowing FAC.

In practical numerical calculations vector components are given at some discrete grid points and the CECS systems are placed at another grid. The elementary systems defined in Eqs. (9) and (10) are singular at the origin, where $\rho' \to 0$. This means that some care must be used, so that the vectors components are not evaluated in the immediate vicinity of the CECS poles. In practice we use interleaved grids, so that vector components are evaluated only at the corners of the CECS grid cells. Our notation is such that the 2-dimensional vector fields (in this example the electric field) are indicated using italics, $\boldsymbol{E}$, as done already in the previous sections. The collection of the x- and y-components of the field $\boldsymbol{E}$ at all grid points is written in script style, as $\boldsymbol{\mathcal{E}}$, and can be written out as

$$\boldsymbol{\mathcal{E}} = \left[E_x(\boldsymbol{r}_1),\ E_y(\boldsymbol{r}_1),\ E_x(\boldsymbol{r}_2),\ \ldots,\ E_y(\boldsymbol{r}_N)\right]^T. \tag{11}$$

Here $E_x(\boldsymbol{r}_n)$ is the x-component of $\boldsymbol{E}$ at the grid point $\boldsymbol{r}_n$, and so on. In a similar fashion the collection of the CECS scaling factors representing the field $\boldsymbol{E}$ is indicated using fraktur style, $\mathfrak{V}$, and is defined as

$$\mathfrak{V} = \left[V^{cf}(\boldsymbol{r}_{p1}),\ V^{df}(\boldsymbol{r}_{p1}),\ V^{cf}(\boldsymbol{r}_{p2}),\ \ldots,\ V^{df}(\boldsymbol{r}_{pM})\right]^T. \tag{12}$$

Here $V^{cf}(\boldsymbol{r}_{pm})$ is the scaling factor of the curl-free CECS located at grid point $\boldsymbol{r}_{pm}$. There is a linear relation between the vector components and the CECS scaling factors,

$$\boldsymbol{\mathcal{E}} = \mathbf{M} \cdot \mathfrak{V}. \tag{13}$$

The matrix $\mathbf{M}$ depends only on the geometry of the vector and CECS grids, and can be calculated using Eqs. (9) and (10).

3.2 Algorithm for numerical calculations

With the elementary systems we can formulate the approach of Sect. 2.2 in a somewhat different way. The goal is to find such a curl-free current system $\boldsymbol{J}_{cf}$ that the sum $\boldsymbol{J} = \boldsymbol{J}_{eq} + \boldsymbol{J}_{cf}$ is consistent with a potential electric field. As before, we assume that the equivalent currents are the same as the divergence-free part of the total currents, $\boldsymbol{J}_{eq} = \boldsymbol{J}_{df}$, which is a good approximation at high geomagnetic latitudes.

We begin by calculating the electric field $\boldsymbol{E}_1$ that is consistent with the equivalent currents. This can be written in form (cf. Eq. 7)

$$\boldsymbol{E}_1 = (\Sigma_P \boldsymbol{J}_{eq} - \Sigma_H \hat{\boldsymbol{e}}_z \times \boldsymbol{J}_{eq})/\Sigma^2, \tag{14}$$

where, as before, $\Sigma^2 = \Sigma_P^2 + \Sigma_H^2$. In general, the electric field $\boldsymbol{E}_1$ is not curl-free and it may be very different from the real electric field $\boldsymbol{E}$. It should also be noted that there may be some regions in the analysis area where $\Sigma_P \approx \Sigma_H \approx 0$, but $\boldsymbol{J}_{eq} \neq 0$. The easiest way to deal with these regions is to simply exclude them from the analysis, as the electric field cannot be determined in such regions.

The next step is to divide the field $\boldsymbol{E}_1$ into curl- and divergence-free parts. As in Eq. (13), there is a linear relation between the vector components and CECS representation of $\boldsymbol{E}_1$,

$$\boldsymbol{\mathcal{E}}_1 = \mathbf{M}_1 \cdot \mathfrak{V}_1. \tag{15}$$

The CECS representation, which also gives the division into curl- and divergence-free parts, is easily obtained by inverting the equation. In the following, we need only the divergence-free part of $\boldsymbol{E}_1$. The corresponding scaling factors of the DF CECS are denoted by $\mathfrak{V}_1^{df}$.

The unknown curl-free part of the ionospheric currents, $\boldsymbol{J}_{cf} = -\nabla\Phi$ in Eq. (6), can be constructed using just CF CECS, as

$$\boldsymbol{\mathcal{J}}_{cf} = \mathbf{N}_{cf} \cdot \mathfrak{I}^{cf}, \tag{16}$$

where vector $\mathfrak{I}^{cf}$ contains the CF CECS scaling factors and matrix $\mathbf{N}_{cf}$ depends only on the geometry of the calculation

grids. The electric field $\boldsymbol{E}_2$ that is consistent with $\boldsymbol{J}_{cf}$ can be calculated as in Eq. (14), just replacing $\boldsymbol{J}_{eq}$ by $\boldsymbol{J}_{cf}$. Because also this inverted Ohm's law is linear, together with Eq. (16) it results in

$$\boldsymbol{\mathcal{E}}_2 = \mathbf{K}_2 \cdot \boldsymbol{\mathfrak{J}}^{cf}, \tag{17}$$

where we have defined a new matrix $\mathbf{K}_2$. Both the electric field $\boldsymbol{E}_2$ and the curl-free currents $\boldsymbol{J}_{cf}$ are unknown, but the matrix $\mathbf{K}_2$ relating them depends just on the structure of the calculation grids and on the conductances, and it can be calculated using Eqs. (14), (9) and (10).

We may further construct a matrix relation similar to Eq. (15), that divides $\boldsymbol{E}_2$ into curl- and divergence-free parts using CECS,

$$\boldsymbol{\mathcal{E}}_2 = \mathbf{M}_2 \cdot \boldsymbol{\mathfrak{V}}_2. \tag{18}$$

Also in this case the matrix $\mathbf{M}_2$ depends only on he geometry of the calculation grids. Now we can use Eqs. (17) and (18) together, and write a relation between the still unknow curl-free currents and CECS representation of the electric field $\boldsymbol{E}_2$,

$$\boldsymbol{\mathfrak{V}}_2 = \mathrm{inv}(\mathbf{M}_2) \cdot \mathbf{K}_2 \cdot \boldsymbol{\mathfrak{J}}^{cf}. \tag{19}$$

In the following calculations we need only the divergence-free part of $\boldsymbol{E}_2$, which is given by the divergence-free CECS $\boldsymbol{\mathfrak{V}}_2^{df}$. This part of the scaling factors may be singled out by picking appropiate rows of the matrix $\mathbf{L}\equiv\mathrm{inv}(\mathbf{M}_2)\cdot\mathbf{K}_2$. Equation (19) can be written out as

$$\begin{pmatrix} V_2^{cf}(\boldsymbol{r}_{p1}) \\ V_2^{df}(\boldsymbol{r}_{p1}) \\ V_2^{cf}(\boldsymbol{r}_{p2}) \\ \vdots \end{pmatrix} = \begin{pmatrix} L_{11} & L_{12} & \dots \\ L_{21} & L_{22} & \dots \\ \vdots & \vdots & \ddots \end{pmatrix} \cdot \begin{pmatrix} I^{cf}(\boldsymbol{r}_{p1}) \\ I^{cf}(\boldsymbol{r}_{p2}) \\ I^{cf}(\boldsymbol{r}_{p3}) \\ \vdots \end{pmatrix}. \tag{20}$$

We see that in this case the divergence-free scaling factors V_2^{df} correspond to the odd rows of the matrix $\mathbf{L}$. By defining a new matrix $\mathbf{L}_{df}$ consisting of the odd rows, we may write a matrix relation between the divergence-free part of the CECS representation of $\boldsymbol{E}_2$ and the curl-free current system,

$$\boldsymbol{\mathfrak{V}}_2^{df} = \mathbf{L}_{df} \cdot \boldsymbol{\mathfrak{J}}^{cf}. \tag{21}$$

If we assume that the total electric field $\boldsymbol{E}=\boldsymbol{E}_1+\boldsymbol{E}_2$ is curl-free, then the rotational parts of $\boldsymbol{E}_1$ and $\boldsymbol{E}_2$ must cancel each other, so that

$$\boldsymbol{\mathfrak{V}}_2^{df} = -\boldsymbol{\mathfrak{V}}_1^{df}. \tag{22}$$

With this condition we can solve the unknown curl-free part of the ionospheric currents as

$$\boldsymbol{\mathfrak{J}}^{cf} = -\mathrm{inv}(\mathbf{L}_{df}) \cdot \boldsymbol{\mathfrak{V}}_1^{df}. \tag{23}$$

As explained above, the vector $\boldsymbol{\mathfrak{V}}_1^{df}$ is obtained from the equivalent currents using Eqs. (14) and (15) and the matrix $\mathbf{L}_{df}$ can be contructed through the steps taken in Eqs. (16–21). After solving Eq. (23) we know the true ionospheric current density $\boldsymbol{J}=\boldsymbol{J}_{eq}+\boldsymbol{J}_{cf}$, and consequently also the electric field can be solved using Eq. (7).

In summary, the calculation algorithm based on the elementary systems is following:

- Calculate the electric field $\boldsymbol{E}_1$ that is consistent with Ohm's law and the equivalent currents.
- Divide $\boldsymbol{E}_1$ into curl- and divergence-free parts.
- Construct a relation between the unknown curl-free part of the current $\boldsymbol{J}_{cf}$ and the electric field $\boldsymbol{E}_2$ consistent with it.
- Solve for $\boldsymbol{J}_{cf}$ using the condition that the total electric field $\boldsymbol{E}_1+\boldsymbol{E}_2$ is curl-free.

This CECS-based calculation algorithm is slightly different from the method presented in Sect. 2.2. For example, in the CECS method we do not have to calculate the gradients of conductances or the curl of the equivalent currents. However, the basic approach of solving the curl-free currents instead of electric potential is the same. In the CECS algorithm we do not have to provide any explicit boundary conditions. The CECS represent the curl and divergence of the vector fields, so the natural and automatically included boundary condition is to assume that the curl and divergence vanish outside the analysis region.

In this article we concentrate on regional studies, but it should be mentioned that the new calculation method can also be used in global scales. The theory presented in Sect. 2.2 does not depend on the specific geometry that is used, and also the numerical algorithm presented in this section can be used in spherical geometry. The necessary modification is to simply use Spherical elementary current systems (SECS, introduced by Amm, 1997) instead of CECS.

4 Results for a simple electrojet

In this section we apply both the traditional KRM method of Sect. 2.1 and the new CECS algorithm presented in Sect. 3.2 to a simple one-dimensional electrojet. The generic electrojet model, illustrated in Fig. 2, is uniform in the y-direction. In the x-direction the electric field, Pedersen conductance and Hall/Pedersen conductance ratio all have a Gaussian profile with a half-width of $\sim$260 km on top of a uniform background. As explained in Sect. 2, the input quantities of the KRM and CECS methods are the Pedersen and Hall conductances together with the equivalent currents. In this model the electric field and the conductance gradients are parallel, which means that the equivalent currents are simply the Hall currents. We also use the correct conductance distributions given in the model, although in real situations accurate estimates are quite hard to obtain.

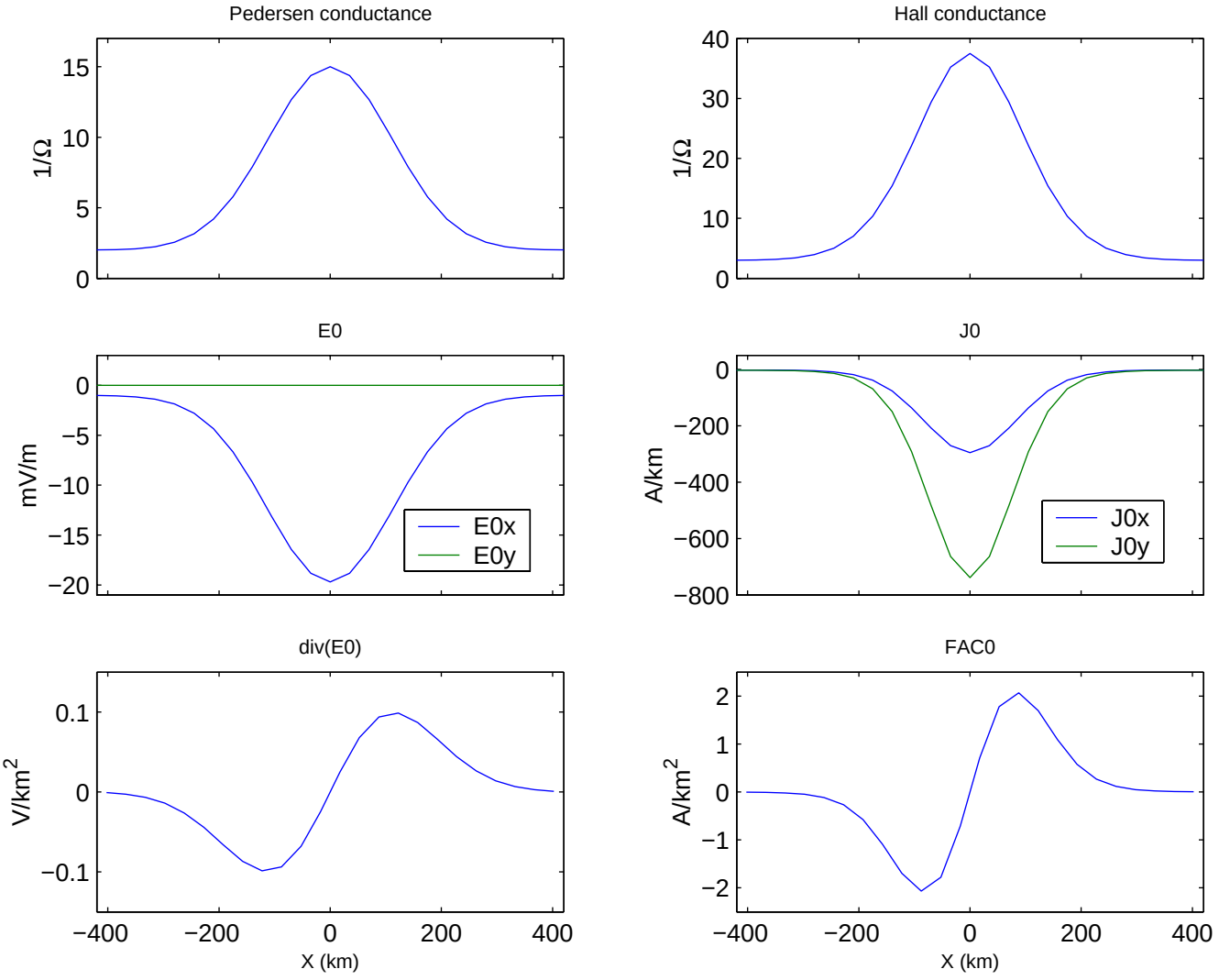

Fig. 2. The electrojet model. Electrojet is uniform in the y-direction. This figure shows the profiles of Pedersen and Hall conductances, electric field $\boldsymbol{E}_0$, ionospheric current density $\boldsymbol{J}_0$, divergence of the electric field and FAC in the x-direction.

Calculations are done in a 25×49 grid, with 35 km and 50 km spacing in x- and y-directions, respectively. The KRM equation Eq. (4) is solved using a finite difference scheme with successive overrelaxation (Press et al., 1992, chapter 19). We use a boundary condition ϕ=0 for the electric potential in the KRM solution. The new CECS based solution is calculated as outlined in Sect. 3.2. The required matrix inversions are calculated using singular value decomposition (Press et al., 1992, chapter 2).

The results of the traditional KRM and the new CECS methods are shown in Figs. 3 and 4, respectively. Both calculation methods produce results that show quite strong boundary effects at the eastern and western sides, where the electrojet is artificially truncated by the boundaries of the calculation area. For that reason we show the results at a smaller area, omitting 300 km of the calculation grid at both ends of the electrojet. For both methods four quantities are shown: the calculated electric field $\boldsymbol{E}$, its divergence $\nabla\cdot\boldsymbol{E}$, the ionospheric sheet current density $\boldsymbol{J}$ and the FAC. For each variable also the difference between the calculated result and the original model is shown.

The electric field at the central electrojet region is reproduced relatively well by the KRM method, but the ϕ=0 boundary condition causes some errors near the northern and southern boundaries. Because all boundaries have the same potential, the line integral of the electric field from the northern to southern boundary must vanish. This is the reason why the KRM electric field in Fig. 3 shows oppositely directed side lobes at the both northern and southern edges of the main jet. Consequently, also the divergence of the electric field shows a similar behavior. In the central part of the electrojet the KRM method gives a good estimate for $\nabla\cdot\boldsymbol{E}$,

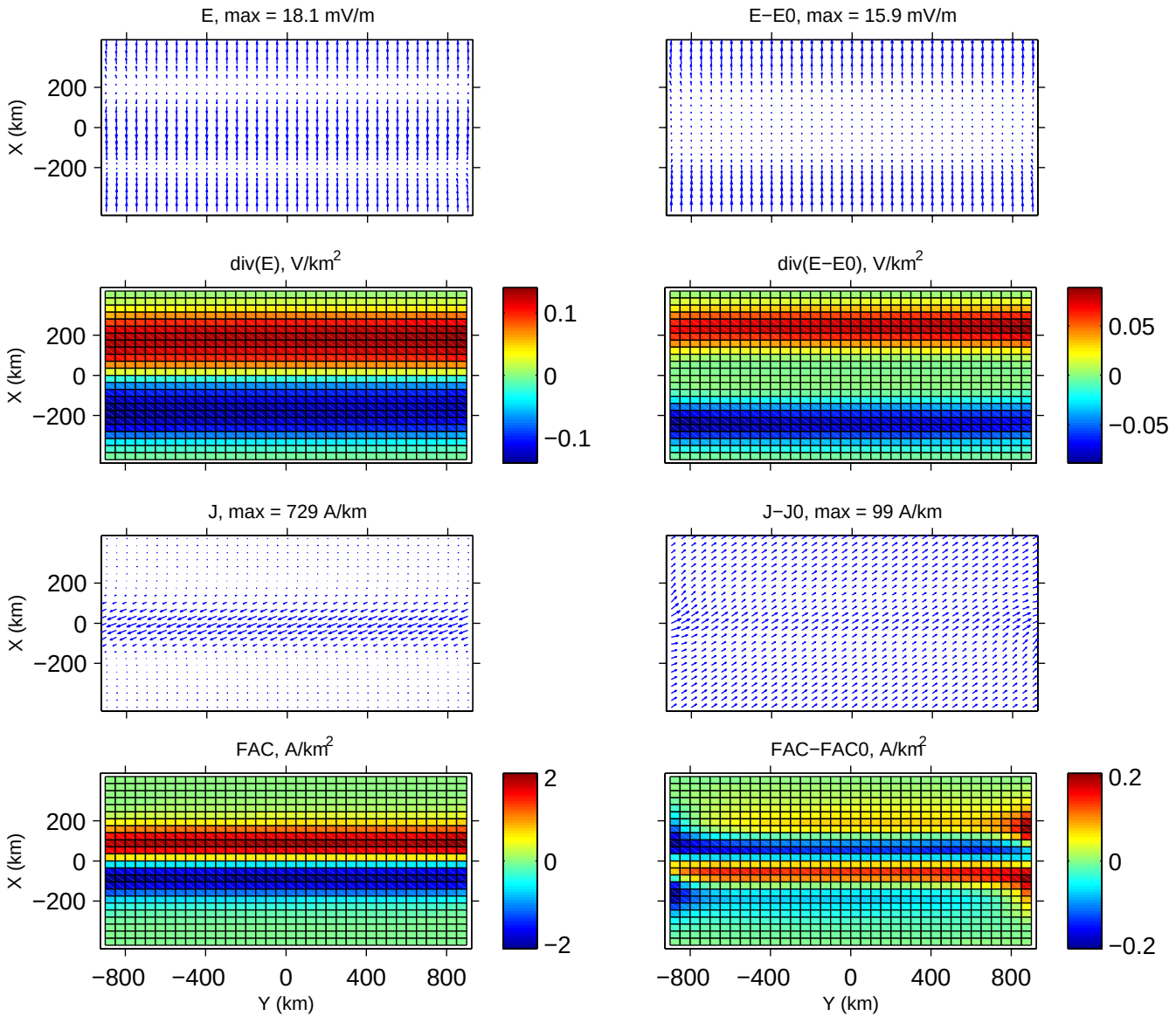

Fig. 3. KRM results for the electrojet model. At each row the KRM result is shown on the left side and the difference between the KRM result and the original model is on the right side. Rows from top to bottom are: electric field, divergence of the electric field, horizontal currents and FAC. Note the different scales of the vector plots.

but the calculated distribution is much wider than the original model, leaking outside the actual electrojet. This example highlights the importance of boundary conditions, when the KRM method is used in local studies. Further examples have been given by Murison et al. (1985). In contrast to the electric field, the horizontal current $\boldsymbol{J}$ and vertical FAC are generated very well by the KRM method. This is understandable, since the currents are concentrated in a narrow strip of enhanced conductivity, where also the electric field was reconstructed accurately. The difference between the KRM result and the original model, $\boldsymbol{J}-\boldsymbol{J}_0$, is an almost uniform North-East directed current, that has magnitude of ∼14% of the main electrojet. The FAC distribution given by the KRM method is slightly too wide and the peak amplitude is about 10% smaller than in the original model, but on the whole the result is good.

The new CECS method is able to reproduce the electric field much more accurately than the KRM method, as can be seen in Fig. 4. The difference to the original model is a relatively uniform, roughly North-West directed component that has a magnitude of ∼20% of the main electrojet field. The divergence of the electric field is also generated very well in the main electrojet area. The largest errors appear at the northern and southern boundaries of the calculation area, and

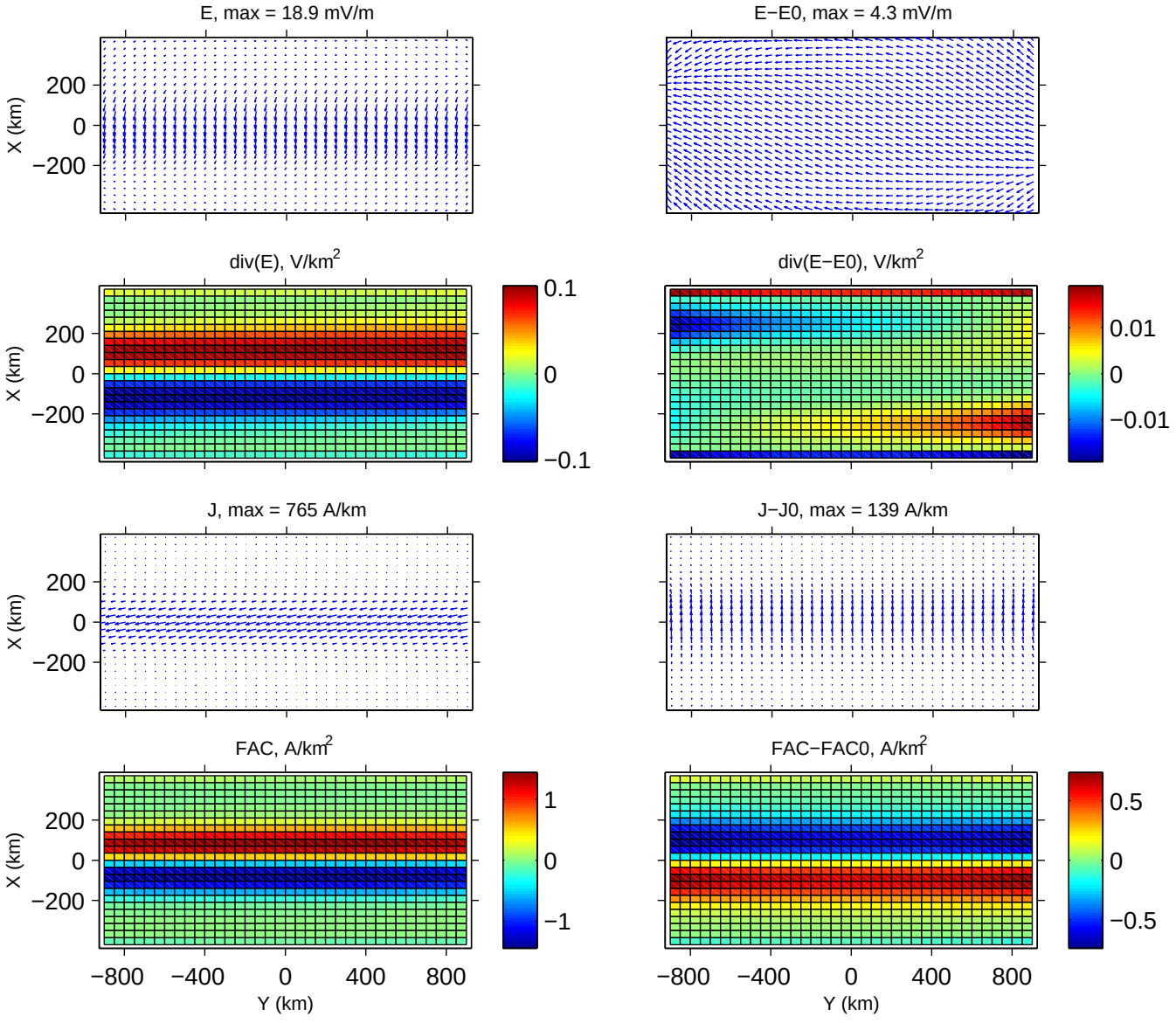

Fig. 4. Results of the CECS method for the electrojet model. Layout is similar to Fig. 3. Note the different scales of the vector plots.

there is also a clear asymmetry in the East-West direction, which results from the sudden termination of the electrojet at these boundaries. However, the current system seems to be reproduced more poorly than with the KRM method. There is about 15% error in the main electrojet current. Main part of the electrojet consists of the Hall currents, which in this case are the same as $\boldsymbol{J}_{eq}$. The Pedersen currents are curl-free and are connected to the FAC system. The CECS method underestimates the divergent Pedersen currents, so that the difference $\boldsymbol{J}-\boldsymbol{J}_0$ points almost directly northward and the FAC given by the CECS method are consistently too small. It should be noted that the CECS basis functions used in this paper are intrinsically 2-dimensional and thus, regardless of the specific application, are not optimally suited for representing 1-dimensional vector fields in a bounded domain. There exists also a 1-dimensional variant of the elementary systems, used by Vanhamäki et al. (2003) and Juusola et al. (2006), which offer a much more suitable set of basis functions for modeling 1-dimensional structures. However, this approach is not pursued further in this study.

From Figs. 3 and 4 it seems that in this simple example the KRM method does produce somewhat better results for $\boldsymbol{J}$ and FAC, while the new CECS method is able to generate $\boldsymbol{E}$ and $\nabla\cdot\boldsymbol{E}$ more accurately. More quantitative estimate for the accuracy of the two methods can be obtained by calculating the mean error in the results, as

$$\text{error(a)} = \frac{\langle |a - a_0| \rangle}{\langle |a_0| \rangle} \cdot 100\% \tag{24}$$

Table 1. Errors in the electrojet results calculated by the KRM and CECS methods. Error is calculated using Eq. (24) and data presented in Figs. 3 and 4.

	$\boldsymbol{E}$	$\nabla\cdot\boldsymbol{E}$	$\boldsymbol{J}$	FAC
KRM	108%	74%	29%	7.5%
CECS	42%	9.1%	24%	40%

Table 2. Errors in the Ω-band results calculated by the KRM and CECS methods. Error is calculated using Eq. (24) and data presented in Figs. 6 and 7.

	$\boldsymbol{E}$	$\nabla\cdot\boldsymbol{E}$	$\boldsymbol{J}$	FAC
KRM	97%	90%	99%	172%
CECS	43%	45%	43%	104%

Here $<>$ denotes average over the calculation area, a is either $\boldsymbol{E}$, $\nabla\cdot\boldsymbol{E}$, $\boldsymbol{J}$ or FAC and a_0 is the corresponding model value.

The error estimates given by Eq. (24) for the electrojet case are given in Table 1. Before discussing these estimates, some important properties of Eq. (24) should be noted. It is easy to see that only the correct solution has 0% error, and a zero solution (e.g. $\boldsymbol{E}$=0) has 100% error. However, some solutions may have errors >100%, but it is questionable whether they are worse than the zero solution. For example a solution that is very close to the correct one, but spatially displaced by just few grid cells may have a very large error as calculated from Eq. (24). With these precautions in mind, Table 1 confirms the previous conclusion that in this example the new CECS method gives more accurate results for the electric field, whereas the current system (especially FAC) is calculated better with the KRM method. The two methods have almost the same percentual errors in the horizontal current $\boldsymbol{J}$, although the plots of $\boldsymbol{J}-\boldsymbol{J}_0$ in Figs. 3 and 4 are quite different.

5 Results for realistic data-based models

In this section we use the KRM and CECS methods with two realistic data-based models, namely the Ω-bands and the westward traveling surge (WTS). These models have been published by Amm (1995) and Amm (1996). They are based on observational data obtained at northern Scandinavia by the Scandinavian Magnetometer Array, the EISCAT radar and the EISCAT magnetometer cross, and the STARE radar.

In these more complicated models we cannot identify $\boldsymbol{J}_{eq}$ with the Hall currents. Instead we calculate the equivalent currents as the divergence-free part of the total ionospheric current density. We divide the total current into divergence- and curl-free parts using the CECS method, as done for the electric field in Sect. 3.2. In order to avoid committing an inverse crime, i.e. using exactly the same numerical process both in preparing the input data and then solving the inverse problem, we use different grid spacings in the separation and in the actual calculations and also add 2% of normally distributed noise to the resulting equivalent (or divergence-free) currents. The original models are given in a regular grids with 50 km resolution in both x- and y-directions. In the separation of the total model current into divergence- and curl-free parts we use 42 km separation for the CECS, but in the actual calculations the original 50 km separation is used.

5.1 Ω-band

The Ω-band model is illustrated in Fig. 5. The model consists of the Pedersen and Hall conductances, the potential electric field $\boldsymbol{E}_0$, the divergence of the electric field and corresponding sheet currents $\boldsymbol{J}_0$ together with the FAC. Numerical calculations are done in the same way as in Sect. 4.

The results obtained using the two methods are given in Figs. 6 and 7. The results are also compared in Table 2, where the error numbers from Eq. (24) are given. In this example the KRM method fails almost completely in generating either the electric field or the horizontal currents, which is again due to the wrong boundary condition. If we want to obtain better results, we must have some additional a priori information about the structure of the electric field, so that better boundary conditions can be chosen. Although the error numbers given in Table 2 for $\nabla\cdot\boldsymbol{E}$ and FAC are very large, these quantities seem to be produced somewhat better than the vector fields. Especially the divergence of the electric field has reasonable resemblance to the original model, at least qualitatively. However, the details are not generated correctly, as the area of negative $\nabla\cdot\boldsymbol{E}$ at the middle of the calculation grid is too weak and slightly misplaced, and the positive divergences at both sides are overestimated. The FAC in the KRM result are mostly concentrated in two small regions, in the same way as in the original model, although neither the exact position nor the magnitude are correct. In the KRM results there are also some weaker and more spread upward and downward FAC areas, that are not present in the original model.

The new CECS based method gives clearly better results, as can be seen in Fig. 7 and in Table 2. The basic shapes of $\boldsymbol{E}$ and $\boldsymbol{J}$ are produced well, although the magnitude and direction of the fields are not quite the same as in the original model. Also $\nabla\cdot\boldsymbol{E}$ and FAC are produced better than with the KRM method, and especially the divergence of the electric field is in quite a good qualitative agreement with the model. The FAC given by the CECS method are less accurate, but also in this case the CECS method seems to give a better result than the KRM method.

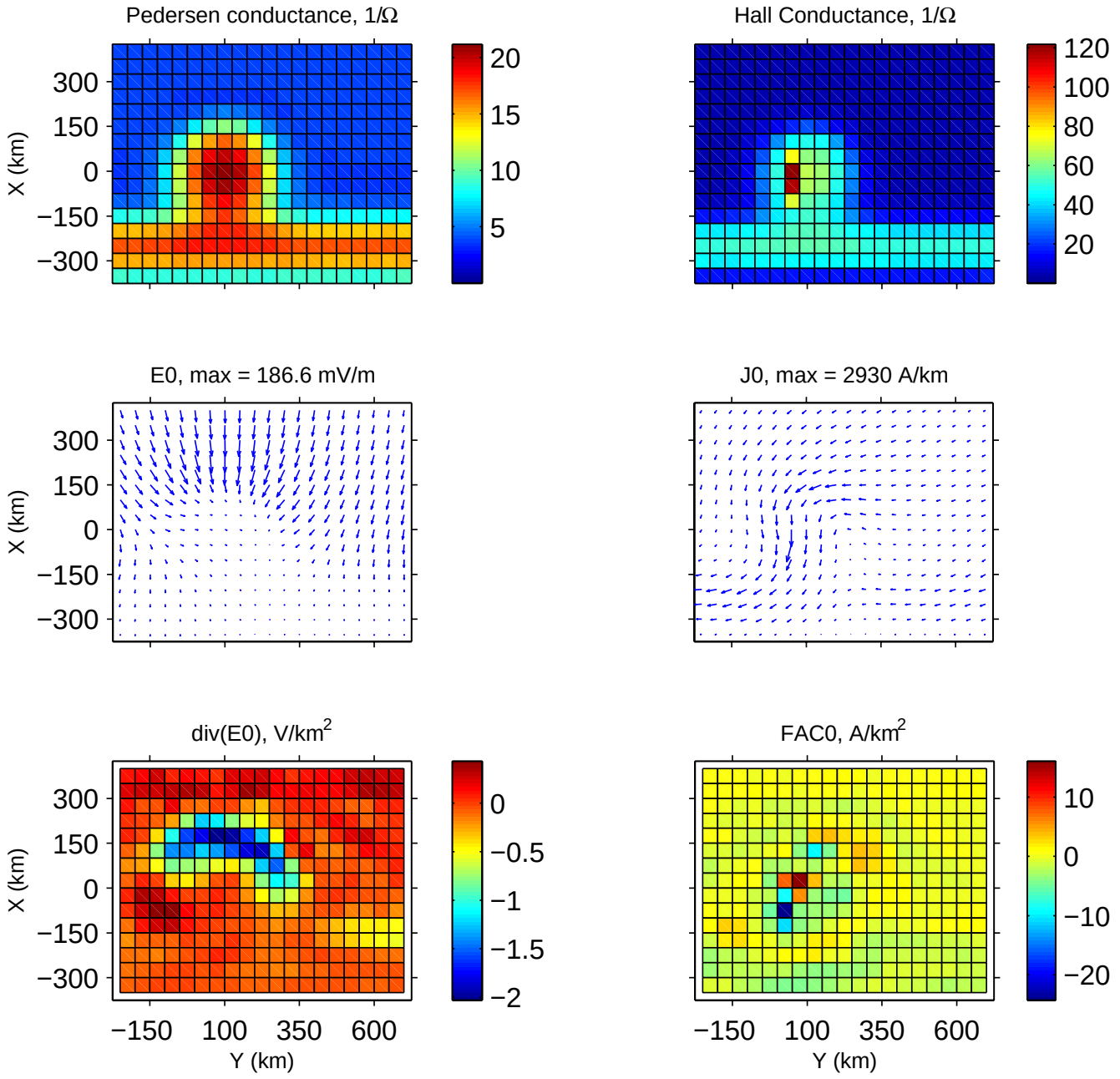

Fig. 5. The Ω-band model. Pedersen and Hall Conductances, electric field $\boldsymbol{E}_0$, ionospheric current density $\boldsymbol{J}_0$, divergence of the electric field and FAC. Note the different scales of the vector plots.

5.2 WTS

The input WTS model is shown in Fig. 8 and the KRM and CECS results are illustrated in Figs. 9 and 10, respectively. The KRM method is able to reproduce the most prominent large scale patterns of $\nabla\cdot\boldsymbol{E}$, $\boldsymbol{J}$ and FAC with some accuracy. However, there are also significant deviations from the original model at some areas and the detailed structure of the WTS system is distorted in the KRM solution. The electric field seems to be reproduced more poorly than the other parameters, at least when judging qualitatively from Fig. 9. The largest errors in $\boldsymbol{E}$ are concentrated near the boundaries and are apparently caused by the incorrect boundary conditions. However, in order to make a better guess at the boundary conditions for the electric potential we would need some additional information about $\boldsymbol{E}$. In this case the largest errors in $\boldsymbol{E}$ are concentrated in areas where conductances are rather small, so the horizontal currents are not affected as much.

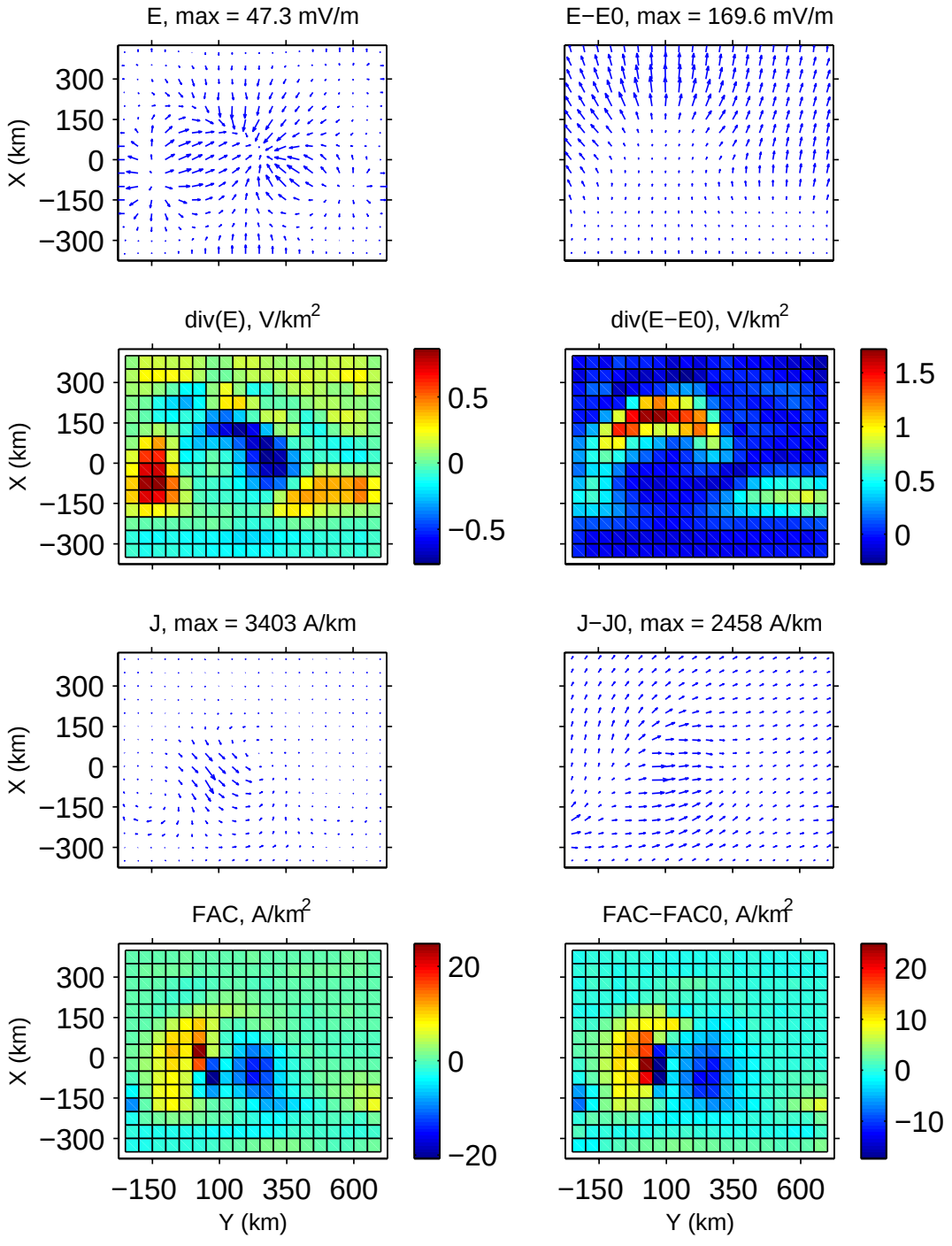

Fig. 6. KRM results for the Ω-band model. Layout is similar to Fig. 3. Note the different scales of the vector plots.

The solution obtained using the new CECS-based method is shown in Fig. 10. Apart from some deviations at the eastern boundary and at the North-West corner the CECS method gives very accurate results. It is clear from Figs. 9 and 10 that the CECS method is able to generate all the parameters more accurately than the KRM method. This is confirmed in Table 3 where the errors calculated using Eq. (24) are given.

The WTS is a very dynamical phenomenon and inductive effects may play a significant role in it, as was reported by Vanhamäki et al. (2007). In these situations the ionospheric electric field is not a pure potential field, as is assumed both in the KRM and CECS methods, but there is also a significant rotational part. This may be taken into account in an approximate way by estimating the rotational electric field using the

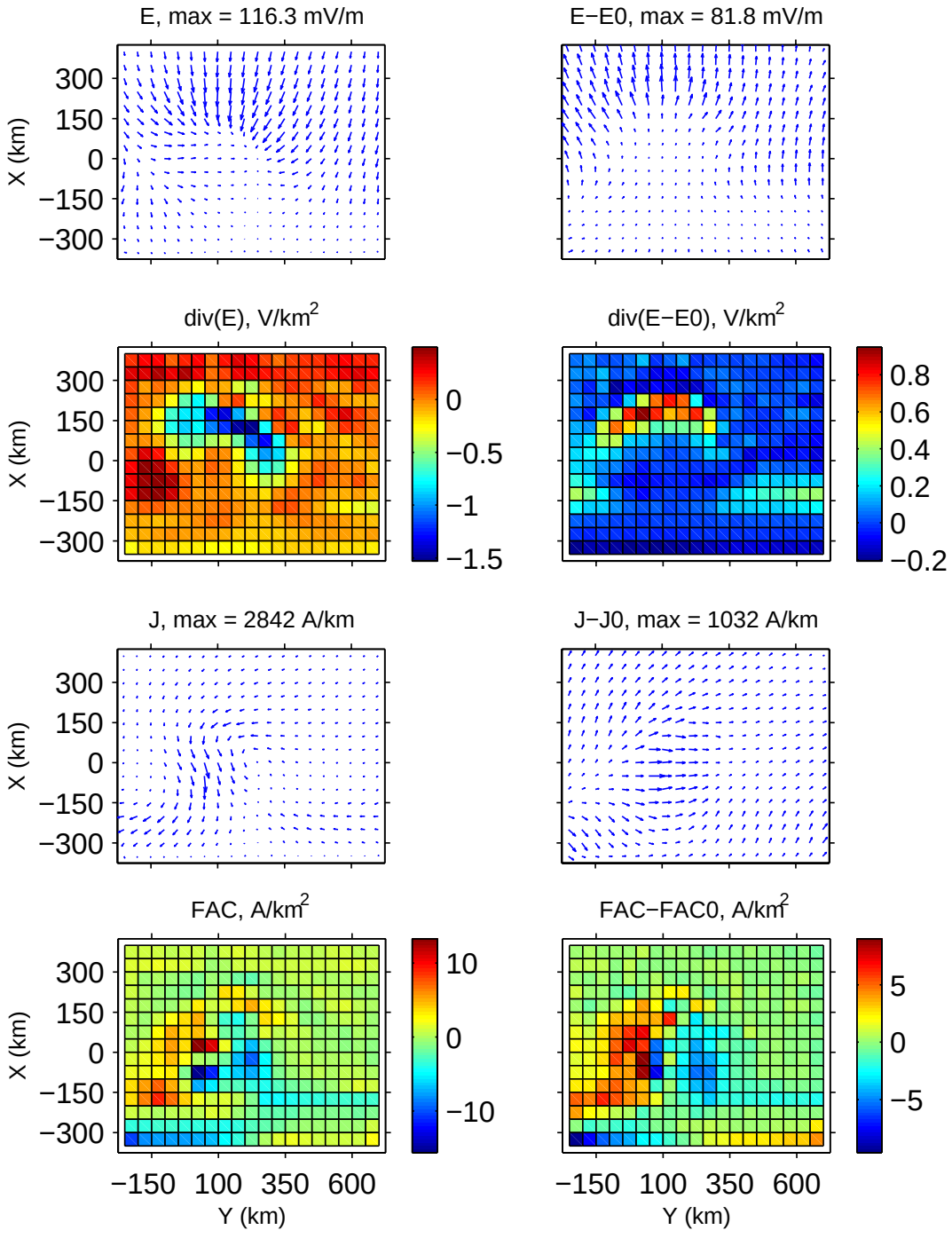

Fig. 7. Results of the CECS method for the Ω-band model. Layout is similar to Fig. 3. Note the different scales of the vector plots.

time derivative of the equivalent currents and then subtracting the inductive part from $\boldsymbol{J}_{eq}$, as discussed in Sect. 2.2 and in Vanhamäki et al. (2007).

6 Summary and conclusions

We have presented a new method for estimating ionospheric electric fields and currents using ground magnetic recordings and ionospheric electric conductances as input data. This problem, using the same set of input data, has traditionally been analyzed using the KRM method introduced by Kamide

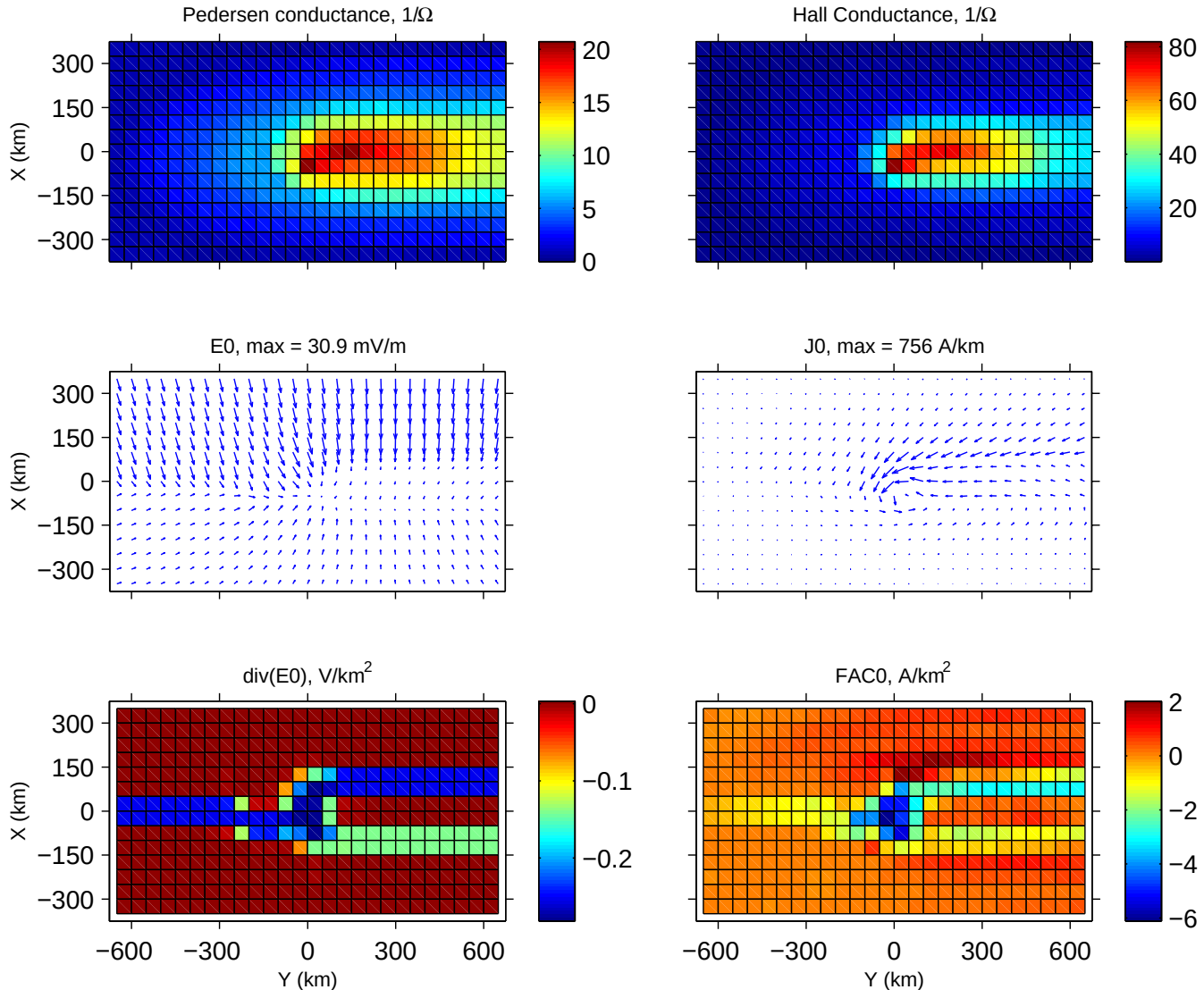

Fig. 8. The WTS model. Layout is similar to Fig. 5. Note the different scales of the vector plots.

et al. (1981). The new method introduced here differs from the KRM method in two important ways. Firstly, the primary unknown to be solved in the new method is the curl-free part of the ionospheric current system, whereas the KRM method formulates the problem in terms of an electric potential. Secondly, in the numerical implementation we use the Cartesian elementary current systems (CECS), that offer a convenient way to represent 2-dimensional vector fields, especially when the vector fields have to be divided into curl- and divergence-free parts. These new features lead to a different formulation of the problem, as explained in detail in Sects. 2 and 3.

In this article we concentrated on regional studies, where magnetic measurements and estimates of the ionospheric conductances are available only at a limited region of few hundred or thousand km across. While the KRM method works well on global and semiglobal scales, at smaller areas the unknown boundary conditions for the electric potential play a significant role in the KRM solution, as was pointed out by Murison et al. (1985). Our approach of solving the curl-free part of the ionospheric current results in an equation

Table 3. Errors in the WTS results calculated by the KRM and CECS methods. Error is calculated using Eq. (24) and data presented in Figs. 9 and 10.

	$\boldsymbol{E}$	$\nabla\cdot\boldsymbol{E}$	$\boldsymbol{J}$	FAC
KRM	80%	169%	51%	52%
CECS	19%	46%	8.8%	17%

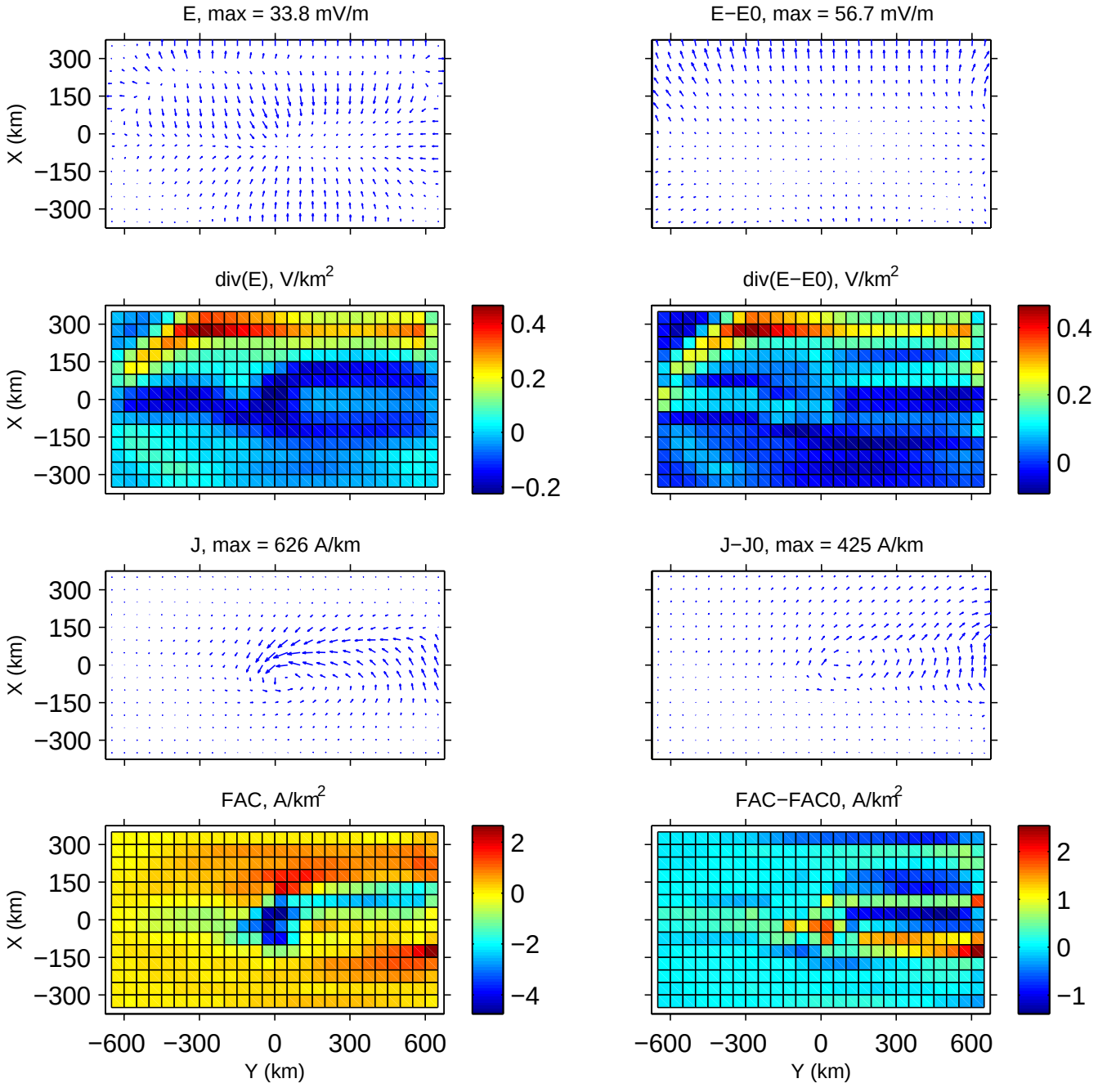

Fig. 9. KRM results for the WTS model. Layout is similar to Fig. 3. Note the different scales of the vector plots.

(Eq. 8) that makes better use of the information contained in the input equivalent currents than the KRM formulation. Another advantage is that with CECS the boundary conditions are implemented in a natural way, without having to specify any explicit values for the vector fields or potentials at the boundaries. Thus we expect the new method to be more suitable for regional studies than the traditional KRM method. The new calculation method may also be used in global studies, as mentioned in Sect. 3.

In Sect. 4 we compared the KRM and CECS methods by analyzing a simple 1-dimensional electrojet model. In Sect. 5 we further applied the two methods to two realistic models of typical meso-scale phenomena in the auroral ionosphere, namely the Ω-bands and the westward traveling surge (WTS). In the electrojet case the result was quite even, as the CECS method produced better estimates for the electric field while the KRM method was able to generate the FAC more accurately. This may be partly explained by the fact that the

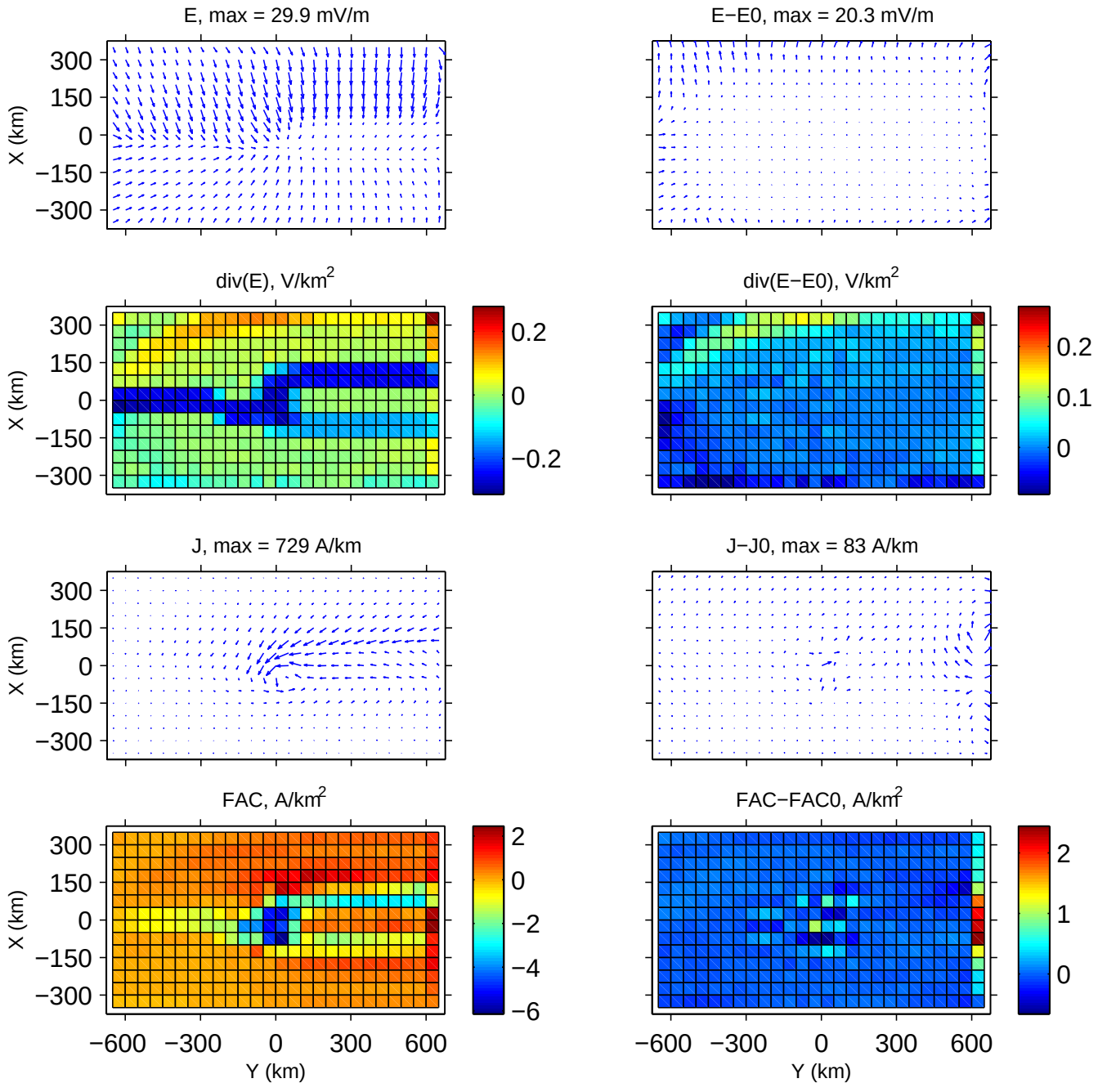

Fig. 10. Results of the CECS method for the WTS model. Layout is similar to Fig. 3. Note the different scales of the vector plots.

CECS basis functions are not optimal for representing essentially 1-dimensional structures, as discussed in Sect. 4. However, in the three data-based test cases, which show full 2-dimensional variability, the new CECS method was clearly superior to the traditional KRM method. The error estimates calculated using Eq. (24) show that the errors in the CECS results are around 20%–40% in the model cases, whereas the errors in the KRM results are significantly larger. However, it should be mentioned that in these examples we used the correct Pedersen and Hall conductance distributions in the calculations. In real situations there may be large uncertainties in the conductance estimates, as discussed in Sect. 2.1. Additionally, in the studied examples the input models had about the same resolution as was used in the calculations, but in reality also much smaller scale variations would be present. These could not be reproduced by neither the KRM nor the new CECS method, nor any by any other method that is based on ground magnetometer input data.

We conclude that the new CECS-based calculation method is well suitable for regional studies and seems to produce more accurate results than the traditional KRM method. One possible topic for a future study is a more thorough comparison between the CECS method and the local AMIE-KRM code mentioned in Sect. 2.1. Also a systematic evaluation of the uncertainties caused by inaccurate conductance estimates would be useful when interpreting the results.

Acknowledgements. The authors would like to thank A. Viljanen for his valuable comments on the manuscript. The work of H. Vanhamäki was supported by the Finnish Graduate School in Astronomy and Space Physics.

Topical Editor M. Pinnock thanks H. Wang and A. Aikio for their help in evaluating this paper.

References

Ahn, B.-H., Richmond, A. D., Kamide, Y., et al.: An ionospheric conductance model based on ground magnetic disturbance data, J. Geophys. Res., 103, 14 769–14 780, 1998.

Aksnes, A., Amm, O., Stadsnes, J., et al.: Ionospheric conductances derived from satellite measurements of auroral UV and X-ray emissions, and ground-based data: A comparison, Ann. Geophys., 23, 343–358, 2005, http://www.ann-geophys.net/23/343/2005/.

Amm O.: Direct determination of the local ionospheric Hall conductance distribution from two-dimensional electric and magnetic field data: Application of the method using models of typical ionospheric electrodynamic situations, J. Geophys. Res., 100, 21 473–21 488, 1995.

Amm, O.: Improved electrodynamic modeling of an omega band and analysis of its current system, J. Geophys. Res., 101, 2677–2683, 1996.

Amm, O.: Ionospheric elementary current systems in spherical coordinates and their application, J. Geomagnetism and Geoelectricity, 49, 947–955, 1997.

Amm, O. and Viljanen, A.: Ionospheric disturbance magnetic field continuation from the ground to the ionosphere using spherical elementary current systems, Earth, Planets Space, 51, 431–440, 1999.

Amm, O., Viljanen, A., Pulkkinen, A., Sillanpää, I., and Vanhamäki, H.: Methods for combined ground-based and space-based analysis of ionospheric current systems, Proc. Fourth Oersted International Science Team Conference, Copenhagen, Denmark, 23–27 September 2002, p. 181–184, 2003.

Chapman, S. and Bartels, J.: Geomagnetism, vol. II, pp. 1049, Oxford University Press, New York, 1940.

Fuller-Rowell, T. J. and Evans, D. S.: Height-integrated Pedersen and Hall conductivity patterns inferred from the TIROS-NOAA satellite data, J. Geophys. Res., 92, 7606–7618, 1987.

Haines, G. V.: Spherical cap harmonic analysis, J. Geophys. Res., 90, 2583–2591, 1985.

Janhunen, P.: Reconstruction of electron precipitation characteristics from a set of multiwavelength digital all-sky auroral images, J. Geophys. Res., 106, 18 505–18 516, 2001.

Juusola, L., Amm, O., and Viljanen, A.: One-dimensional elementary current systems and their use for determining ionospheric currents from satellite measurements, Earth, Planets Space, 58, 667–678, 2006.

Kamide, Y., Richmond, A. D., and Matsushita, S.: Estimation of ionospheric electric fields, ionospheric currents, and field-aligned currents from ground magnetic records, J. Geophys. Res., 86, 801–813, 1981.

Kamide, Y., Kihn, E. A., Ridley, A. J., Cliver, E. W., and Kadowaki, Y.: Real-time specifications of the geospace environment, Space Sci. Rev., 107, 307–316, 2003.

Lummerzheim, D., Rees, M. H., Craven, J. D., and Frank, L. A.: Ionosheric conductances derived from DE-1 auroral images, J. Atmos. Terr. Phys., 53, 281–289, 1991.

Murison, M., Richmond, A. D., Matsushita, S., and Baumjohann, W.: Estimation of Ionospheric Electric Fields and Currents From a Regional Magnetometer Array, J. Geophys. Res., 90, 3525–3530, 1985.

Press W. H., Teukolsky, S. A., Vetterling, W. T., and Flannery, B. P.: Numerical Recipes in Fortran 77, 973 pp., Campridge University Press, Cambridge, 2nd ed., 1992.

Pulkkinen, A., Amm, O., Viljanen, A., and BEAR Working Group: Ionospheric equivalent current distributions determined with the method of spherical elementary current systems, J. Geophys. Res., 108(A2), 1053, doi:10.1029/2001JA005085, 2003.

Untiedt, J. and Baumjohann, W.: Studies of polar current systems using the IMS Scandinavian magnetometer array, Space Sci. Rev., 63, 245–390, 1993.

Richmond, A. D. and Kamide, Y.: Mapping electrodynamic features of the high-latitude ionosphere from localized observations: Technique, J. Geophys. Res., 93, 5741–5759, 1988.

Vanhamäki H., Amm, O., and Viljanen, A.: One-dimensional upward continuation of the ground magnetic field disturbance using spherical elementary current systems, Earth, Planets Space, 2003.

Vanhamäki H., Amm, O., and Viljanen, A.: Role of inductive electric fields and currents in dynamical ionospheric situations, Ann. Geophys., 25, 437–455, 2007, http://www.ann-geophys.net/25/437/2007/.